Volume 13
Number 1
January 2026
Pages 1–670

Environmental Science Nano

rsc.li/es-nano

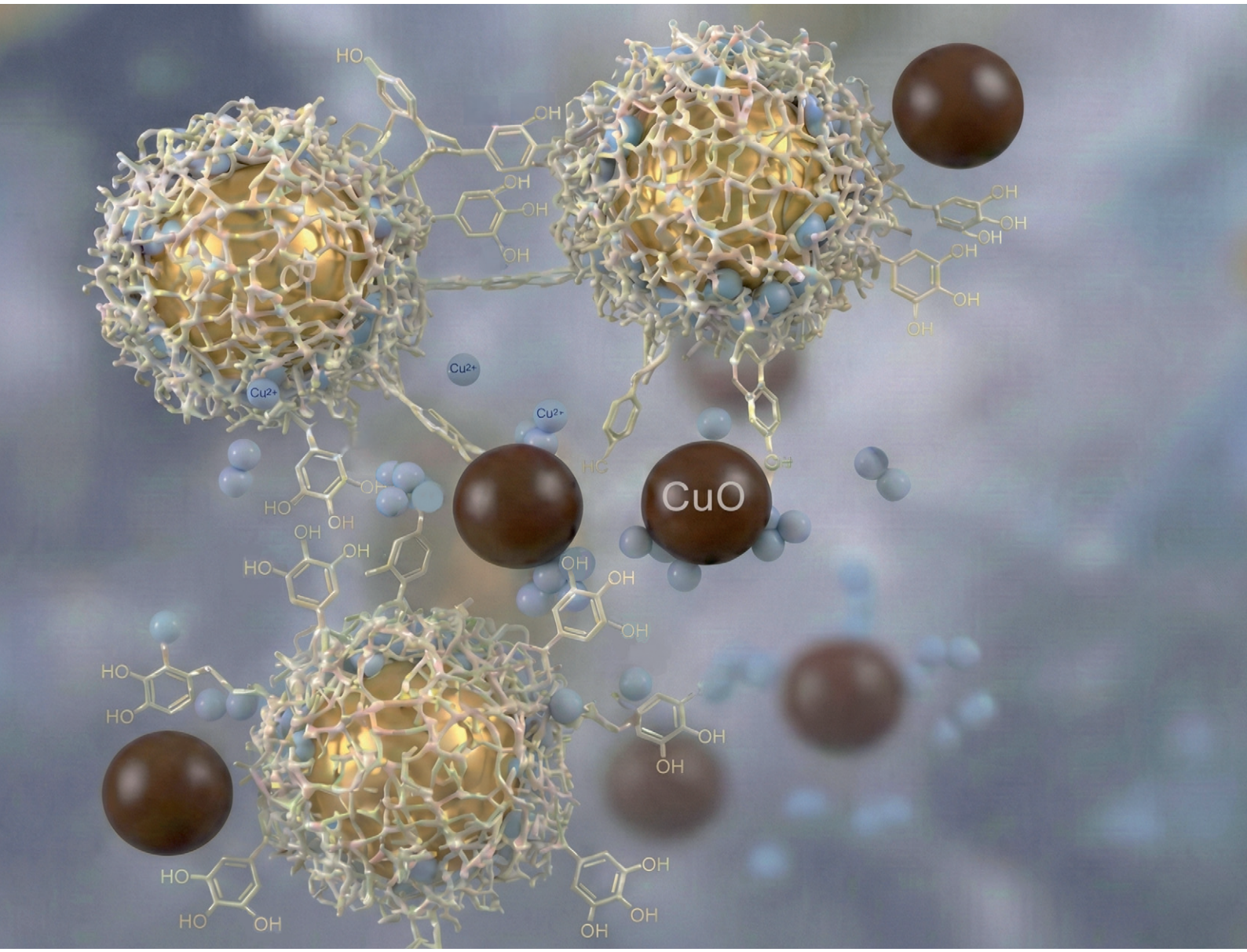

ISSN 2051-8153

ROYAL SOCIETY OF CHEMISTRY

PAPER
Monika Mortimer *et al.*
Metal–phenolic network-coated nanoparticles mitigate CuO nanotoxicity

Environmental Science Nano

ROYAL SOCIETY OF CHEMISTRY

PAPER

View Article Online
View Journal | View Issue

Cite this: *Environ. Sci.: Nano*, 2026, **13**, 242

Metal–phenolic network-coated nanoparticles mitigate CuO nanotoxicity

Anett Välimets, [ab] Danylo Merzhyievskyi, [a] Ilona Juvonen, [ac] Karin Valmsen, [a] Isabelle Worms, [d] Vera I. Slaveykova, [d] Asya Drenkova-Tuhtan, [a] Nicholas Andrikopoulos, [ae] Pu Chun Ke, [e] Anne Kahru [a] and Monika Mortimer *[a]

Received 28th April 2025,
Accepted 19th November 2025

DOI: 10.1039/d5en00428d

rsc.li/es-nano

Copper is widely used to control various plant diseases and recent trends highlight the prominence of copper-based nanomaterials in developing new nanoagrochemicals. As these nanomaterials eventually end up in the aquatic environment, they necessitate increased attention regarding their environmental and human health risks. Herein, we demonstrate the use of metal–phenolic network (MPN) nanocomposites as novel agents for mitigating the toxicity of copper oxide (CuO) nanoparticles (NPs), which exert toxicity mainly through released Cu ions. Iron–tannic acid-based porous 3D networks on gold NP cores (Fe–TA@Au NPs) exhibited the capacity to reduce CuO NP toxicity in freshwater protozoa *Tetrahymena thermophila* – a model for environmental toxicity, and in human macrophages – an *in vitro* model for human safety. In the macrophage assays, Fe–TA@Au NPs increased the half-effective concentration (EC_{50}) of CuO NPs by approximately three-fold, from 4.7 mg L^{-1} to 15.4 mg L^{-1}. This mitigation occurred through two main mechanisms: adsorption of Cu ions, released from CuO NPs, and reduction of intracellular reactive oxygen species, both of which contributed to the toxicity of CuO NPs. The maximum adsorption capacity for Cu^{2+} was 172 mg g^{-1} of Fe–TA MPN, comparable to other copper adsorbents, including MPNs and metal–organic frameworks (MOFs). Additionally, Fe–TA@Au NPs demonstrated excellent biocompatibility and ecosafety in a highly sensitive microalgal growth inhibition assay and exhibited long-term efficacy, indicating the strong potential of these porous materials in mitigating copper toxicity. Furthermore, the gold NP cores in the MPN model used in this study can easily be replaced with other core NP materials, making them suitable for large-scale environmental and human health applications.

Environmental significance

The development of nanomaterial-based agrochemicals is a growing trend that raises concerns about environmental pollution. Metallic nanomaterials, such as CuO nanoparticles, pose significant risks as they can release toxic copper ions, which are particularly harmful to aquatic ecosystems. Therefore, it is essential to establish effective strategies to mitigate the environmental and health risks associated with nanomaterials. One of the most cost-effective methods for removing toxic metal ions is adsorption. This study explores the use of novel adsorbents, metal-phenolic networks, for their environmental safety and effectiveness in reducing the toxicity of CuO nanoparticles.

1. Introduction

The global nanomaterials market, valued at 8.5 billion USD in 2019, is expected to grow at a compound annual growth rate of 13% from 2020 to 2027.[1] In terms of nanoparticle (NP) applications, medical fields, electronics, and paints & coatings account for the majority of the global market share.[2] Traditionally, copper-based nanomaterials have been mainly used as electrical conductors, but their applications, including CuO NPs, are rapidly expanding into new areas such as agriculture,[3] including organic farming, and, owing to their antimicrobial properties, in food preservation, textiles, coatings, and water treatment.[4] Additionally, CuO

[a] *Laboratory of Environmental Toxicology, National Institute of Chemical Physics and Biophysics, Akadeemia tee 23, 12618 Tallinn, Estonia. E-mail: monika.mortimer@kbfi.ee*
[b] *School of Natural Sciences and Health, Tallinn University, Narva mnt. 25, 10120 Tallinn, Estonia*
[c] *Department of Chemistry and Biotechnology, School of Science, Tallinn University of Technology, Ehitajate tee 5, Tallinn 19086, Estonia*
[d] *Environmental Biogeochemistry and Ecotoxicology, Department F.-A. Forel for Environmental and Aquatic Sciences, Faculty of Sciences, University of Geneva, Bvd Carl-Vogt 66, 1211-Geneva, Switzerland*
[e] *Drug Delivery, Disposition and Dynamics, Monash Institute of Pharmaceutical Sciences, Monash University, 381 Royal Parade, Parkville, VIC 3052, Australia*

NPs are incorporated into innovative adsorbents and catalytic composite materials for pollutant degradation and sorption.[5] Through these applications, the environment, natural and drinking water, and humans are inevitably exposed to CuO NPs, which highlights the need to consider potential health hazards associated with these nanomaterials.

Although the bioactivity of CuO NPs makes them beneficial for certain environmental applications, they have also been associated with toxicity in "non-target" organisms such as invertebrates, fish, and mammals, including humans.[6] Copper is also a well-known algicide and CuO NPs are used in antifouling paints for marine vessels.[7] Additionally, the European Commission's Scientific Committee on Consumer Safety has raised concerns over the use of copper-based nanomaterials in cosmetics due to the potential of NPs being absorbed through the skin or mucous membrane. Toxicity studies in environmentally relevant test species and mammalian cells *in vitro* have indicated that the main mechanisms of toxicity for CuO NPs include (i) dissolution of NPs and (ii) cellular uptake of NPs followed by dissolution and induction of oxidative stress and consequent cellular damage.[8–12] Released metal ions from NPs may exert toxicity by interacting with metal-binding functional groups of proteins and enzymes or by interfering with the cellular electron transport chain and redox processes, resulting in elevated reactive oxygen species (ROS) levels and oxidative stress. Thus, dissolution of NPs contributes to ROS production (*e.g.*, involving Fenton-like reactions), but may also proceed through NP interactions with the cellular components. For example, for protozoa *Tetrahymena thermophila*, the half-lethal (LC_{50}) values of Cu ions are at low, ~0.01–2 mg L^{-1} level,[11,13] while for mammalian cells, the median LC_{50} is ~10–100 mg L^{-1}.[6] The higher LC_{50} values observed in mammalian cell cultures may be attributed to the lower bioavailability of Cu in the protein-rich culture medium, as Cu toxicity has been correlated with the organic compound content in the test media.[14] Therefore, reducing the levels of bioavailable dissolved Cu ions could provide opportunities for mitigating the toxicity of CuO NPs.

Several strategies have been employed to modify the properties of nanomaterials to reduce their toxicity. Reduction of NP solubility by surface modifications has been successfully used to design safer NPs. For example, Fe-doping reduced Cu ion shedding by the formation of a stable $CuFe_2O_4$ phase at the CuO NP surface.[15] Also, natural compounds such as dissolved organic matter (DOM) have been shown to reduce the toxicity of soluble NPs.[9,16–18] The proposed strategies of modifying NP chemistry and surface structure for safer NPs can be effective in the design phase of novel materials. However, to address the concerns about the contamination of NPs already released into the environment or NPs internalized by organisms, effective metal and NP-sequestrating agents are necessary. Adsorption is a facile and cost-effective method for heavy metal removal.[19] The most commonly explored adsorbents for heavy metal removal from polluted water include activated carbon, graphene, Fe-based nanomaterials, and low-cost natural inorganic materials such as clays, minerals, apatites and iron oxides, as well as organic materials like cellulose, alginate, chitosan, and biochars from different feedstocks.[19] Although the low cost and natural availability of some of these adsorbents are beneficial, their adsorption capacity and affinity for metals are often limited. This typically requires the use of high amounts of adsorbents, which raises concerns about the safe disposal of metal-laden materials. Therefore, there is a need for new, efficient, and biocompatible metal adsorbents for use in water treatment and *in vivo* applications. For instance, a recent study showed that metal ion sequestration by functional amyloids effectively reduced metal oxide NP toxicity *in vivo*.[20]

The aim of this study was to demonstrate that polyphenol tannic acid – (TA) and Fe^{3+}-based metal–phenolic networks (MPNs) can reduce the toxicity of CuO NPs by acting as efficient copper adsorbents in aquatic environments. Recently, MPNs have gained increasing attention as adsorbent materials[21,22] and both TA and Fe^{3+} are generally recognized as safe (GRAS) by the U.S. FDA.[23] Furthermore, Fe–TA MPNs have been demonstrated to be biocompatible in NIH-3T3 fibroblasts[24] and in mice.[25] To enhance adsorption capacity, MPNs can be synthesized on nanoparticulate substrates to produce nanocomposite materials with a larger specific surface area compared to micro- or macro-sized MPNs.[26] In the current study, Au NP cores were coated with layers of Fe–TA MPNs (rendering Fe–TA@Au NPs). The nanocomposites were characterized using ultraviolet-visible (UV-vis) spectroscopy, dynamic light scattering (DLS), transmission electron microscopy (TEM), Fourier-transform infrared spectroscopy (FTIR), total reflection X-ray fluorescence (TXRF) spectrometry and asymmetric flow field-flow fractionation (AF4). Their biocompatibility was evaluated using free-living freshwater heterotrophic protozoan *T. thermophila*, microalgal growth assays, and human macrophages *in vitro*. Bioassays demonstrated that Fe–TA@Au NPs effectively reduced the toxicity of CuO NPs and Cu^{2+}. The underlying mechanisms of toxicity mitigation were examined, based on the hypothesis that the galloyl and catechol functional groups in the Fe–TA MPN are potent metal ion coordinators and the fact that TA is a robust antioxidant. Thus, both Cu ion adsorption and intracellular ROS reduction by Fe–TA@Au NPs were investigated. The results suggest a potential new application of MPNs in detoxifying copper-based nanomaterials and copper. Additionally, the study demonstrates the use of biotests for evaluating both biocompatibility and the effectiveness of novel materials, thereby supporting a safe-by-design approach in developing functional nanocomposites.

2. Materials and methods

2.1. Synthesis of metal–phenolic network-coated nanoparticles (Fe–TA@Au NPs)

Fe–TA@Au NPs were synthesized essentially as reported earlier with slight modifications.[27] Briefly, Au NPs were first

synthesized using TA as a reducing and particle-stabilizing agent. Before each synthesis, the beaker and the stir bar were rinsed with *aqua regia*. A 50 mL glass beaker containing 4.7 mL ultrapure water (Direct-Q® Water Purification System, Merck Millipore) and a stir bar were placed on a magnetic stir plate, set to 40 °C, and stirred at 300 rpm. Then 100 μL of TA (ACS reagent, Sigma Aldrich) solution in ultrapure water (10 mg mL^{-1}) was added and stirred for 15 min. Two hundred μL of 10 mM $HAuCl_4$ ($HAuCl_4{\cdot}3H_2O$, ≥99.9% trace metals basis, Sigma-Aldrich) was then dropwise added and the dark red suspension, indicative of Au NP formation, was stirred for another 15 min. To remove excess TA, the Au NP suspension was centrifuged at 13 000*g* for 10 min, the supernatant was removed and the pellet resuspended in 5 mL ultrapure water. Centrifugation was repeated to wash Au NPs with water. To synthesize the Fe–TA coating on Au NPs, 0.8 mL of the Au NP suspension with an optical density at 530 nm (OD_{530}) ~ 1 was pipetted into a 1.5 mL microcentrifuge tube, 4.08 μL TA at 10 mg mL^{-1} was added and mixed by vortexing for 10 s, followed by the addition of 10 μL of 2.4 mM $FeCl_3$ solution ($FeCl_3{\cdot}6H_2O$, ACS reagent, Sigma-Aldrich) and vortexing for 10 s. To facilitate the formation of Fe–TA MPN, the pH of the mixture was adjusted by adding 200 μL of 50 mM Tris-HCl buffer (pH 8, Sigma 7-9® tris(hydroxymethyl)aminomethane, ≥99% and HCl, ≥37%, Puriss. p.a ACS reagent from Honeywell Fluka™) and vortexing for 40 s. The mixture was centrifuged at 13 000*g* for 10 min, the supernatant was removed and the pellet was resuspended by vortexing in 0.8 mL ultrapure water. The described steps of adding TA, $FeCl_3$ and Tis-HCl buffer, vortexing and centrifugation were repeated thrice to ensure a thick layer of Fe–TA network on the Au NP cores. Finally, Fe–TA@Au NPs were washed again with ultrapure water by centrifugation, resuspended in 0.8 mL water, and stored in the dark at 4 °C until analysis.

2.2. Nanomaterials and their stock suspensions

CuO NP powder was purchased from Sigma-Aldrich (nanopowder, <50 nm particle size, 29 m^2 g^{-1}, product #544868). The physicochemical properties of CuO NPs were measured in a previous study.[12] CuO NPs were suspended in ultrapure water at 2 g L^{-1} by probe sonication (40 W, Branson Digital Sonifier 450D, USA). The stock suspension was stored in the dark at room temperature. Before each experiment, the stock was resuspended by probe sonication and used for preparing dilutions for testing.

2.3. Characterization of Fe–TA@Au NPs and nanomaterials

For TEM imaging of Au NPs and Fe–TA@Au NPs, suspensions of NPs were dropped on carbon-coated grids, negatively stained with uranyl acetate, and examined with a Tecnai G2 Spirit BioTwin microscope (FEI, USA). TEM image analysis for quantification of Au NP diameters and Fe–TA layer thickness was done using ImageJ software (National Institutes of Health, NIH, Bethesda, MD); 134 Au NP cores and 54 Fe–TA layers were analyzed in the TEM images. UV-vis spectroscopy of Au NPs, Fe–TA@Au NPs and TA was conducted using a Multiskan Spectrum instrument (Thermo Fisher Scientific, Finland) and 1 mL quartz cuvettes. Attenuated total reflection (ATR)-FTIR spectra were obtained using an IRAffinity-1S spectrophotometer (Shimadzu Europa GmbH) with the Quest ATR accessory from Specac (Orpington, UK). TA was analyzed as a powder while 5 μL of Au NP and Fe–TA@Au NP suspension were airdried on the ATR crystal before analysis. The hydrodynamic size and ζ-potential of Au NPs, Fe–TA@Au NPs and CuO NPs (at 100 mg L^{-1}) were measured in ultrapure water and/or in 10 mM 4-(2-hydroxyethyl)piperazine-1-ethanesulfonic acid (HEPES) buffer (pH 7.4, Gibco 15630) using a Zetasizer Nano-ZS (Malvern Instruments, Malvern, UK). The size and metal composition of Au NPs and Fe–TA@Au NPs were also analyzed using an AF4 with a diode array detector (DAD) and inductively coupled plasma mass spectrometry (ICP-MS), as described previously[28,29] and in the SI. Dissolved Cu in CuO NP suspensions and unbound Cu in Fe–TA@Au NP suspensions mixed with $CuSO_4$ (anhydrous, reagent grade, 98.5–100.5%, Alfa Aesar™) or CuO NPs were quantified using TRXF Picofox S2 (Bruker AXS Microanalysis GmbH) or colorimetric bicinchoninic acid (BCA) assay,[30] described in the SI. The experimental data of Cu adsorption were fitted using the Freundlich and Langmuir adsorption isotherms (method in the SI).

2.4. Viability tests with protozoa *Tetrahymena thermophila*

T. thermophila strain BIII, isolated from Protoxkit F™ (MicroBioTests Inc., Nazareth, Belgium), was cultivated axenically as described previously[11] and detailed in the SI. For toxicity testing, protozoa were harvested from Dryl's medium by centrifugation (1000*g*, 5 °C, 10 min) and resuspended in the test medium (either ultrapure water or 10 mM HEPES buffer, pH 7.4). Cell density in the suspension was adjusted to 10^6 cells per mL based on cell counting using a hemocytometer. For counting, cells were fixed in 5% formaldehyde. Protozoa were exposed to test chemicals and NPs in transparent 96-well microplates where 100 μL of chemical solution or NP suspension were mixed with 100 μL protozoan culture per well, resulting in a cell density of 5 × 10^5 protozoa per mL in the test. Wells containing protozoa in ultrapure water or HEPES buffer were used as controls, *i.e.*, as a reference for calculating the % viability in chemical-exposed protozoan samples. The microplates were incubated at 30 °C for 2, 4 or 24 h and then the viability was determined by quantifying the ATP content in the wells. ATP was extracted from the samples by using 4% trichloroacetic acid (TCA) in 4 mM ethylenediaminetetraacetic acid (EDTA) disodium salt dihydrate and ATP was quantified using the ATP Bioluminescent Assay Kit (Sigma-Alrich) as described previously.[31,32] Luminescence emission was quantified using an Orion II plate luminometer (Berthold

Detection Systems, Germany). Dose–response curves were modeled and effective concentrations were calculated using Microsoft Excel macro REGTOX.[33]

2.5. Growth inhibition assessment using unicellular green algae *Raphidocelis subcapitata*

The algal growth assay was performed following OECD guideline 201 (ref. 34) as described previously.[32] The detailed method is available in the SI.

2.6. THP-1 cell line culturing and toxicity testing

THP-1 cells (ATCC) were grown in RPMI 1640 medium with L-glutamine (Corning), supplemented with 10% fetal bovine serum and 1% penicillin and streptomycin (all purchased from Sigma-Aldrich), in 75 cm^2 cell culture flasks (37 °C, 5% CO_2). The cells were subcultured at least twice in suspension and then seeded to 96-well plates at a density of $\sim 1.5 \times 10^5$ cells per mL with at least 98% viability. Cells were differentiated into macrophage-like cells in a 50 nM phorbol 12-myristate 13-acetate (PMA, Sigma-Aldrich)-supplemented culture medium over 48 h. Then, the PMA-containing medium was replaced with a fresh culture medium and the cells were recovered for 24 h. The cells were then exposed to CuO NPs with and without added Fe–TA@Au NPs for 24 h. $NiCl_2{\cdot}6H_2O$ (99.9% trace metals basis, Sigma Aldrich) was used as a positive control, and ultrapure water was used as a negative (vehicle) control. All the samples and concentrations were tested in six replicate wells and three independent experiments were conducted. The viability of the cells was measured fluorometrically using the CellTiter-Blue® Cell Viability Assay kit (Promega). After 24 h exposure, cells were washed twice with culture medium, 100 μL of culture medium in each well was then supplemented with CellTiter-Blue® Reagent (20 μL per well), and the plates were incubated for 4 h before fluorescence measurement (excitation at 560 nm and emission at 590 nm) using a Fluoroskan Ascent FL plate reader (Thermo Labsystems, Helsinki, Finland). Wells containing NPs in a culture medium (but without cells) were included in the test plates to check for any interference of the materials with the fluorescence of the CellTiter-Blue® Reagent. The cells were visualized using an Axio Vert.A1 inverted microscope equipped with a camera Axiocam 208 (Zeiss, Germany).

2.7. CuO NP and $CuSO_4$ toxicity mitigation by Fe–TA@Au NPs

Copper toxicity mitigation assays were performed using *T. thermophila* and THP-1 cell line-derived macrophages. The test protocols followed those described in sections 2.4. for protozoa and 2.6. for THP-1 macrophages. Dilutions of CuO NPs and $CuSO_4$ were prepared at the respective effective concentrations for protozoa or THP-1 derived macrophages, based on viability assays. For toxicity mitigation tests, each CuO NP or $CuSO_4$ dilution was supplemented with freshly synthesized Fe–TA@Au NPs at final concentrations of 50 mg L^{-1} (for protozoan assays) or 100 mg L^{-1} (for THP-1 assays) immediately before adding to the protozoa or macrophages. Exposures were conducted, and viability was measured as described in sections 2.4 and 2.6.

2.8. Quantification of bioavailable copper using recombinant bacteria

The bioavailable Cu in the medium after exposure of protozoa to CuO NPs, $CuSO_4$ and their combinations with Fe–TA@Au NPs was quantified using recombinant *Escherichia coli* MC1061 (pSLcueR/pDNPcopAlux).[35] The bioluminescence of this bacterial strain is proportional to the intracellular Cu ions that bind to a protein that regulates the promoter of the luminescence-encoding gene cassette *luxCDABE*. A constitutively luminescent strain of *E. coli* MC1061 (pDNlux) was used as a reference to determine the levels of Cu that were inhibitory to bacterial bioluminescence due to toxicity. Samples for tests with recombinant sensor bacteria were prepared as described previously.[11] Briefly, protozoa were exposed to CuO NPs and $CuSO_4$ at their respective EC_{50} and EC_{80} concentrations with and without Fe–TA@Au NPs in 24-well plates, with a sample volume of 1 mL per well. Plates were incubated at 30 °C for 2 h. Then, the protozoa were pelleted by centrifugation (1000*g*, 5 °C, 10 min) and the supernatant was collected and filtered through 0.1 μm pore-size syringe filters. The filtrates were mixed in a ratio of 1 : 1 with pre-grown recombinant *E. coli* MC1061, suspended in 0.9% NaCl supplemented with casamino acids (1 g L^{-1}) and glucose (1 g L^{-1}) in the wells of a white 96-well microplate. The microplate was incubated at 30 °C for 2 h before measuring bacterial bioluminescence using an Orion II plate luminometer (Berthold Detection Systems, Germany). Bioavailable Cu concentrations were determined based on a calibration curve generated by plotting the luminescence of sensor bacteria against the known Cu^{2+} (added as $CuSO_4$ and assumed to be 100% bioavailable) concentrations in their exposure media.

2.9. Quantification of intracellular reactive oxygen species (ROS)

Intracellular ROS was quantified using 2′,7′-dichlorofluorescein-diacetate (DCFH-DA, Life Technologies). For that, protozoa were exposed to H_2O_2 or $CuSO_4$ and THP-1 macrophages to CuO NPs with and without Fe–TA@Au NPs in a 96-well microplate as described above. For ROS quantification, 100 μL of each protozoan sample was pipetted into a black 96-well microplate and 10 μL of 1 mM DCFH-DA was added to the samples. In the case of THP-1 macrophages, 25 μL of 0.5 mM DCFH-DA was added to the microplate wells after viability measurements using CellTiter-Blue® Reagent. The plates were incubated at 25 °C (protozoa) or 37 °C, 5% CO_2 (THP-1 macrophages) for 1 h before measuring the fluorescence of dichlorofluorescein (DCF) using a Fluoroskan Ascent FL microplate reader (Thermo Labsystems, Helsinki, Finland) at excitation/emission wavelengths of 485/527 nm.

Intracellular ROS in protozoa was visualized using a confocal laser scanning microscope as described in the SI.

2.10. Statistical analysis

Statistically significant differences were determined by one-way ANOVA and *post hoc* Tukey's multiple comparisons test or Student's *t*-test. Data are presented as mean values ± standard deviations (STDEV). Results were considered significantly different at p-value <0.05.

3. Results and discussion

3.1. Physico-chemical characteristics of the synthesized Fe–TA@Au NPs

For the synthesis of Fe–TA@Au NPs, we applied a core–shell approach, where tannic acid was used as a reducing and a capping agent in the synthesis of Au NPs (Fig. 1a), yielding spherical NPs with a diameter of 25.2 ± 7.5 nm (Fig. 1b and c). Au NPs were then used as cores for synthesizing Fe–TA MPN coatings (Fig. 1a) that appeared as light layers around the dark Au NP cores as captured by TEM (Fig. 1b) and were determined to be, on average, 7.7 ± 3.3 nm thick (Fig. 1d). The formation of the Fe–TA layer on Au NPs was also indicated by the red-shift of the Au NP characteristic peak in the UV-vis absorption spectrum (530 nm to 540 nm, Fig. 2a), attributable to diminished surface plasmon resonance (SPR) of Au NPs due to modified surface properties and the size of NPs.[36] The appearance of a redshift in the absorption peak after capping Au NPs with Fe–TA MPN was consistent with an earlier study where Fe–TA@Au NPs were synthesized by a similar three-layer procedure.[26] Also, the hydrodynamic diameter of Fe–TA@Au NPs increased compared to Au NPs (Fig. 2b), further indicating successful capping of the Au NPs. The size distribution of NPs was additionally explored using an AF4 analysis, which confirmed the monodispersity of Au NPs with an elution profile as a Gaussian peak, centered at a retention time of 8 min (Fig. 2c). Conversely, Fe–TA@Au NPs were eluted as a bi-

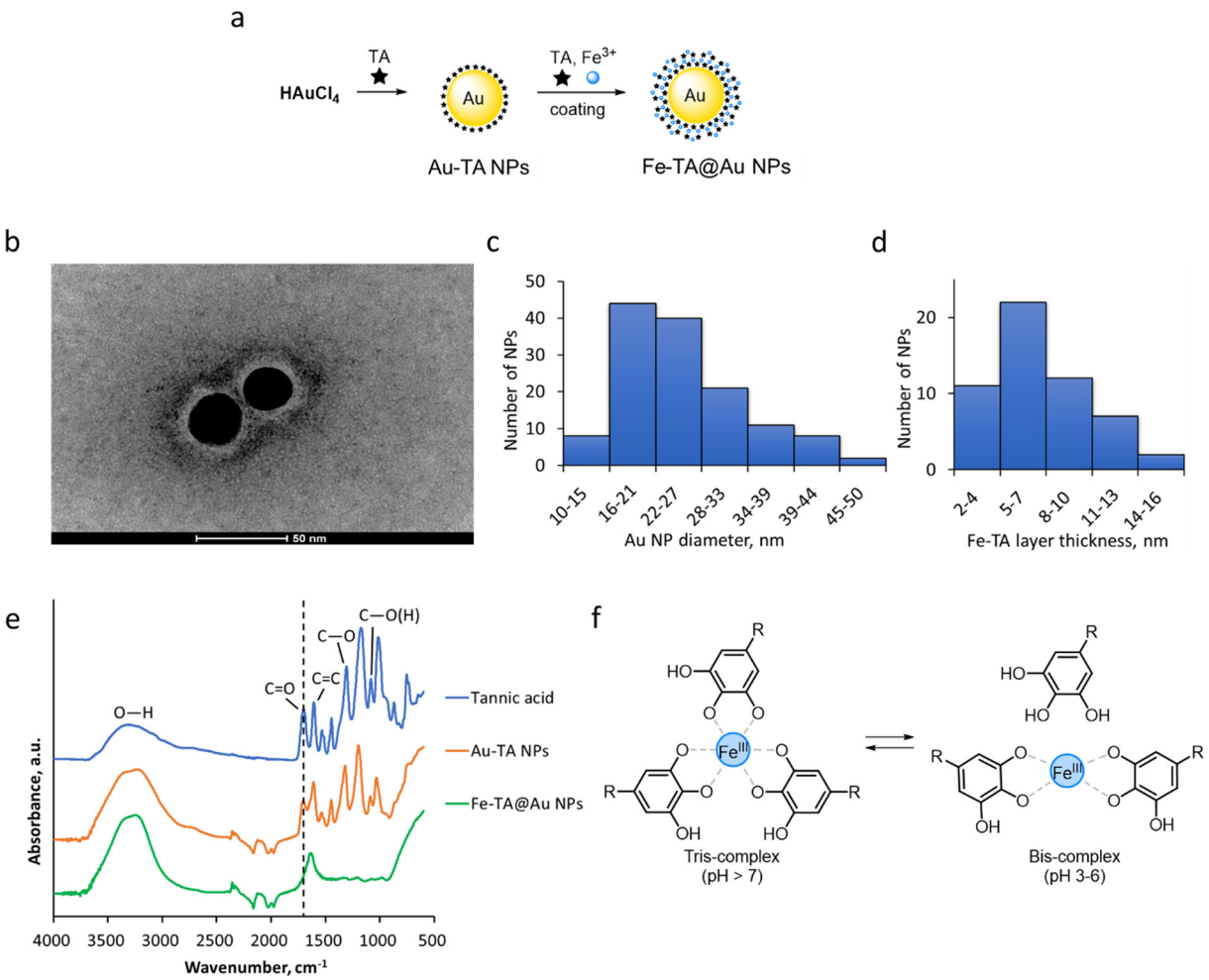

Fig. 1 Physico-chemical characteristics of Fe–TA@Au NPs. (a) Schematic representation of the two-step synthesis of Fe–TA@Au NPs; (b) TEM image of Fe–TA@Au NPs; (c) size distribution of Au NPs cores; (d) distribution of Fe–TA layer thickness around Au NP cores, measured from TEM images; (e) FTIR spectra of tannic acid, Au–TA NPs and Fe–TA@Au NPs; the vertical dashed line indicates the peak corresponding to C=O stretching in the TA spectrum to illustrate the corresponding peak shift to lower wavenumbers in the Fe–TA@Au NPs spectrum; (f) schematic illustration of potential coordination between TA and Fe^{3+} depending on the solution pH.

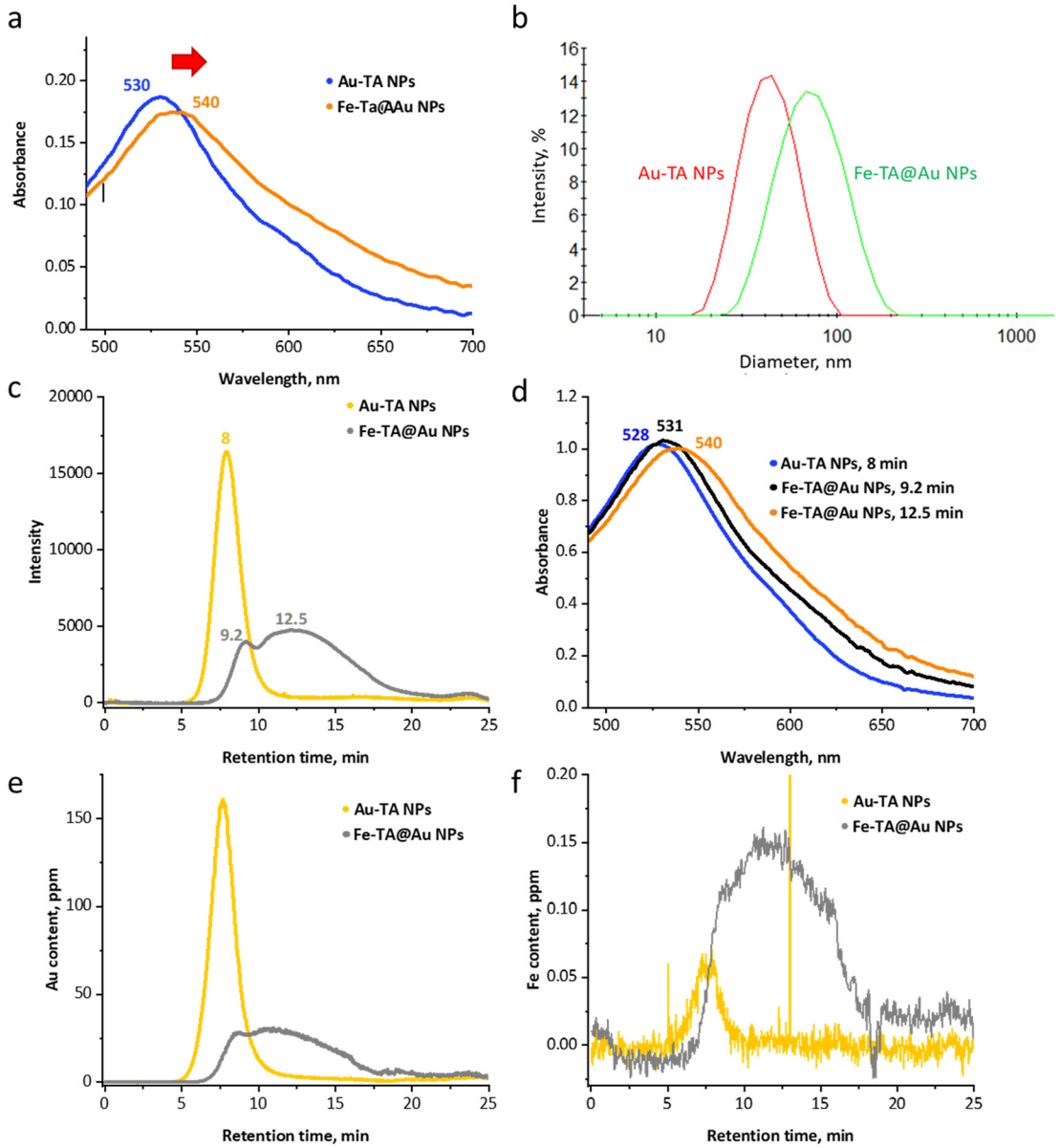

Fig. 2 Spectrophotometric and hydrodynamic properties and elemental composition of Au NPs and Fe–TA@Au NPs. (a) UV-vis spectra of TA-stabilized Au NPs (Au–TA NPs) and Fe–TA@Au NPs suspended in ultrapure water; (b) distributions of the hydrodynamic diameters of Au–TA NPs and Fe–TA@Au NPs suspended in ultrapure water; (c) AF4-DAD fractograms of Au NPs and Fe–TA@Au NPs based on the absorption at 530 nm; (d) UV–vis spectra of Au NPs eluting in AF4 at 8 min and Fe–TA@Au NPs eluting at 9.2 and 12.5 min; (e) AF4-ICP-MS fractograms of Au in Au NPs and Fe–TA@Au NPs; (f) AF4-ICP-MS fractograms of Fe in Au NPs and Fe–TA@Au NPs.

modal population, with longer retention times than Au NPs, consistent with the larger hydrodynamic diameter of the nanocomposites due to the coating of Fe–TA network around the Au NPs (Fig. 2b). The first peak eluted at 9.2 min within the higher size end of the Au NPs, and the main population peak of Fe–TA@Au NPs was centered at 12.5 min (Fig. 2c). Using external calibration (Fig. S1), the hydrodynamic diameter of Au NPs was determined by AF4 as 42 nm, and the main population of Fe–TA@Au NPs was 77 nm. These results are in relatively good agreement with the DLS values, considering the different measurement principles of the two techniques. The SPR signals obtained by direct flow injection analysis (FIA, not shown) and absorbance analysis in AF4 showed maximum bands at 528 nm and 540 nm for Au NPs and Fe–TA@Au NPs, respectively (Fig. 2d), which were similar to the absorbance properties of the NP suspensions in UV-vis analysis (Fig. 2a). AF4 coupled with ICP-MS indicated that the Au signal of Au NPs followed the same elution profile as in DAD (Fig. 2c and e). Similarly, the Au profile of Fe–TA@Au NPs followed its DAD signal, suggesting Fe–TA network association with Au NPs throughout the heterogeneous sample. The Au concentration was similar in Au NP and Fe–TA@Au NP samples, indicating that no significant amount of Au NPs was lost during the synthesis of Fe–TA@Au NPs

(Table S1). The recovery of Au in the AF4 channel was high for Au NPs (92% compared to the Au content of the NP suspension), confirming that Au NPs did not associate with the AF4 membrane, while it was relatively low for Fe–TA@Au NPs (74% of Au was eluted after fractionation), indicating stronger interaction of Fe–TA-coated NPs with the AF4 membrane. The relative instability of the Fe–TA network in the AF4 channel was also confirmed by the low recovery of Fe (44% of the Fe content in the Fe–TA@Au NP suspension). This is expected due to the weak interactions between metal ions and the galloyl groups of tannic acid. Even though the analysis was conducted in HEPES buffer at pH 7 which should maintain Fe in tris-complex with TA (Fig. 1f), interactions with the AF4 membrane and applied crossflow may have compromised the stability of the Fe–TA network but may not be reflective of the Fe–TA@Au NP stability in the suspension.

Indeed, as confirmed by the DLS analysis, the facile synthesis yielded a stable suspension of Fe–TA@Au NPs in water with a hydrodynamic size of 59.8 ± 0.6 nm and a ζ-potential of −44.5 ± 1.0 mV. The suspension stability was maintained once the Fe–TA@Au NPs were suspended in physiologically relevant HEPES buffer (10 mM, pH 7.4) as inferred by the hydrodynamic size of 60.4 ± 0.3 nm and a ζ-potential of −40.0 ± 3.2 mV in the buffer. The MPN-coated NPs did not agglomerate in aqueous suspension for at least four days (Fig. S2). The stability of Fe–TA@Au NPs was also confirmed by measuring TA release, which was ∼5% (in HEPES buffer) and ∼10% (in ultrapure water) of the MPN TA content over 24 h of shaking at room temperature. The TA content was quantified by UV-vis spectroscopy using TA calibration curves (Fig. S3 and S4). The coordination of Fe with the functional groups of TA in the MPN was assessed by ATR-FTIR spectroscopy. While the spectrum of TA-stabilized Au NPs displayed most of the characteristic peaks of TA functional groups (C–O stretching at 1170 and 1305 cm^{-1}, aromatic C═C stretching at 1444 cm^{-1}, and conjugated C═O stretching at 1699 cm^{-1}),[37,38] the coordination of Fe^{3+} by TA in Fe–TA@Au NPs significantly reduced the intensity of the spectrum between the wavenumbers of 100 and 1700 cm^{-1} while broadening the peaks (Fig. 1e). The peak around 1699 cm^{-1}, indicative of C═O stretching of carbonyl groups in the polyphenol molecule, shifted to 1620 cm^{-1} in Fe–TA@Au NPs, indicative of interaction between Fe^{3+} and the phenolic hydroxyl groups that influenced C–O bond stretching vibration, probably due to electron density withdrawal and conjugated electron deficiency. The increased intensity in the O–H stretching at around 3300 cm^{-1} in the Fe–TA@Au NP spectrum compared to the TA spectrum may indicate the residual moisture in the Fe–TA@Au NP material.

3.2. Biocompatibility of Fe–TA@Au NPs in protozoa *T. thermophila* and THP-1-derived macrophages

The biocompatibility of Fe–TA@Au NPs was tested in freshwater free-living ciliate *T. thermophila*, an environmentally relevant organism. *T. thermophila*, as a unicellular eukaryotic organism that feeds by phagocytosis, has proven to be a good test organism for NP biological effect studies due to the capacity of NP internalization by the cells and the ensuing dynamic internal as well as external membrane exposure to NPs.[12,31,39] The exposure of protozoa to Fe–TA@Au NPs was conducted either in ultrapure water (pH ∼ 6) or HEPES buffer (pH 7.4) to exclude the interference of complex media components and to test the impact of pH on the biological effects of Fe–TA@Au NPs. Acute exposure for 24 h indicated that the MPN nanocomposites did not affect the protozoan viability (Fig. 3a) despite being taken up by phagocytosis into the protozoan food vacuoles (Fig. 3b). Although not measured in the current study, *T. thermophila* is known to traffic the content of food vacuoles through the cell and release the contents with a total intracellular processing time of 30 min to 2 h.[40] Thus, the Fe–TA@Au NPs may not have accumulated in the cells, a process that is NP-specific as reported earlier.[31] It was also determined that the components of MPNs (TA and Fe) were not lethal in the concentration range relevant to the MPN construct (Fig. S5), ensuring that the degradation of MPNs in the environment would not pose toxicity. This is consistent with the reported toxicity of Fe to *T. thermophila* (EC_{50} values ∼7.5 mg Fe L^{-1}) under similar exposure conditions (*i.e.*, either in ultrapure water or mineral medium for 24 h)[32,41] which is about fifteen times the Fe concentration in MPNs in the current study (∼0.5 mg L^{-1}). At the highest TA concentration tested in this study (153 mg L^{-1}) about 75% of protozoa were viable (data not shown), indicating that the potentially toxic levels of TA were at least an order of magnitude greater than the TA concentrations in the MPNs (∼15 mg L^{-1}). Also, the protozoan *Euglena gracilis* was recently shown to tolerate well the formation of a Fe–TA MPN layer on the cell surface, not affecting the viability or cell division of the photosynthesizing microorganism.[42] This indicates the excellent biocompatibility of the Fe–TA-based MPNs in single-celled aquatic organisms.

The Fe–TA@Au NP biocompatibility was further confirmed in human THP-1 cell-derived macrophages. The highest concentration of Fe–TA@Au NPs tested was twice as much as in the protozoan test, and these levels were not toxic to THP-1 macrophages as the viability of the Fe–TA@Au NP-exposed cells did not differ significantly from that of the control cells in the pure medium (Fig. 3c). Previously, hollow capsules of Fe–TA MPNs with a diameter of 1 μm, designed for pulmonary deposition, were shown to be non-toxic to human carcinomic alveolar basal epithelial cells (A549) and preferentially associate with alveolar macrophages upon *in vivo* lung deposition.[25] Still, the uptake into macrophages did not induce lung inflammation or toxicity. Here, Fe–TA@Au NP uptake by THP-1-derived macrophages was not quantified, but their association was evident from optical differential interference contrast (DIC) microscopy imaging (Fig. 3d), with no adverse effect on the cell viability.

To further confirm the biocompatibility of Fe–TA@Au NPs, their effects on the growth of microalgae *R. subcapitata*

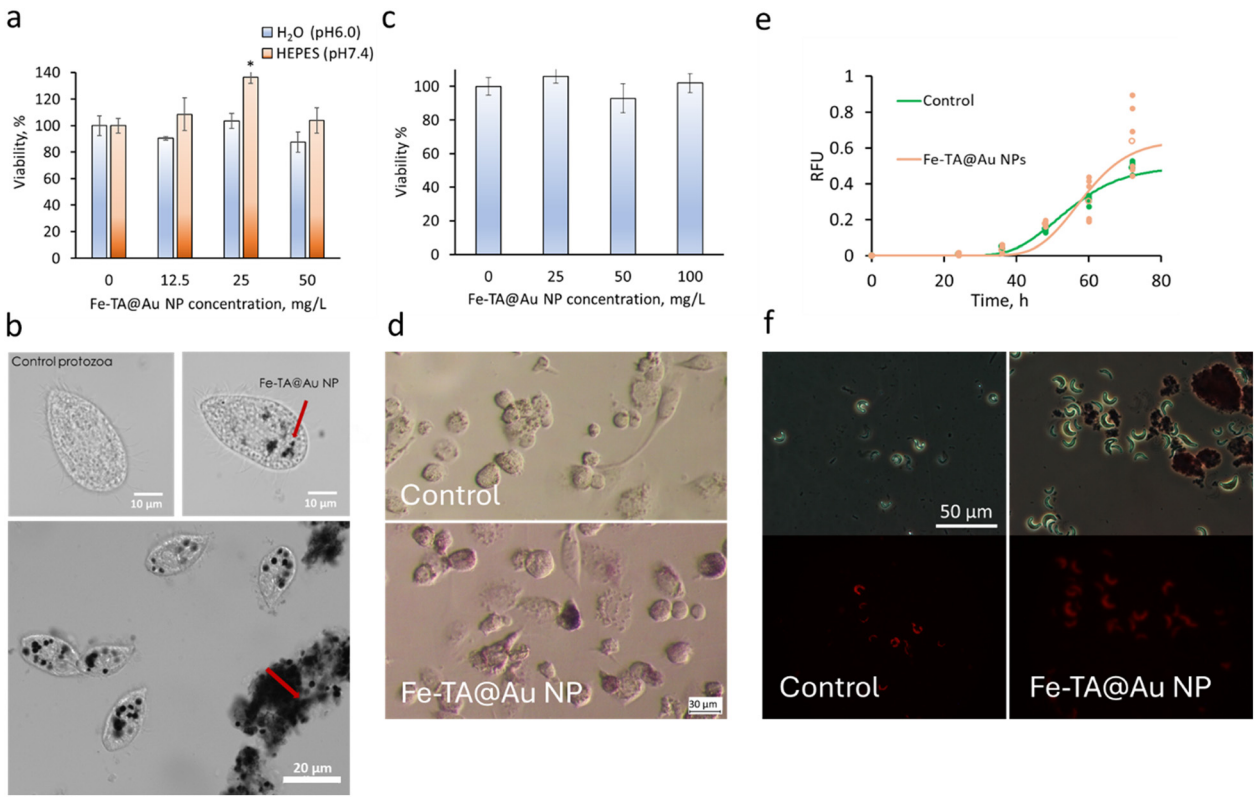

Fig. 3 Biocompatibility and ecosafety of Fe–TA@Au NPs. (a) Relative viability of protozoa *T. thermophila* upon 24 h exposure to Fe–TA@Au NPs at different concentrations in ultrapure water, pH ~ 6.0 or 10 mM HEPES buffer, pH 7.4; (b) bright-field microscopy images of *T. thermophila* incubated in ultrapure water (control protozoa) or water containing 50 mg L^{-1} Fe–TA@Au NPs for 2 h, 30 °C; the red arrows indicate food vacuoles or phagosomes filled with Fe–TA@Au NPs inside the protozoan cell (upper right image) and outside the cells after excretion (lower image); (c) relative viability of THP-1 macrophages exposed to Fe–TA@Au NPs in RPMI 1649 medium for 24 h, 37 °C; (d) optical microscopy images of control THP-1 macrophages (upper image) and 100 mg L^{-1} Fe–TA@Au NP-exposed THP-1 macrophages (lower image). The protozoan images were captured using a black and white camera, while THP-1 derived macrophages were imaged in color. (e) Growth of *R. subcapitata* control and 50 mg L^{-1} Fe–TA@Au NP-exposed cultures. Algal biomass was quantified by extracted chlorophyll fluorescence measurements (RFU – relative fluorescence units). Replicate data were fitted to a logarithmic (log-normal) model using MS Excel macro REGTOX. (f) Phase-contrast (upper images) and fluorescence (lower images) microscopy images of microalgae in control culture and 50 mg L^{-1} Fe–TA@Au NP-exposed cultures after 72 h.

were tested. Toxicity assessments with microalgae are among the recommended methods for regulatory classification of chemicals because of microalgae's high sensitivity to chemicals, especially toward heavy metals, *e.g.*, copper.[32,43] The results showed that Fe–TA@Au NPs at 50 mg L^{-1} did not impact algal growth, as the specific growth rates in the Fe–TA@Au NP-exposed and unamended control cultures were not significantly different (0.09 ± 0.0004 h^{-1} *versus* 0.1 ± 0.007 h^{-1}, Fig. 3e). Phase-contrast microscopy revealed slight hetero-agglomeration of algae with Fe–TA@Au NPs; however, the cells remained viable, as indicated by the presence of red autofluorescence (Fig. 3f). Since the algal growth assay is conducted over 72 h under illuminated conditions, Fe–TA@Au NPs may release Fe ions from the MPN structure during the test. Still, even in the worst-case scenario where the MPN structures fully degrade, the released Fe ion concentration at a maximum of 0.5 mg L^{-1} (in the case of 50 mg L^{-1} Fe–TA@Au NPs) would not inhibit the growth of *R. subcapitata*, as shown in tests with $FeCl_3$ where no growth inhibition occurred at 5 or 10 mg L^{-1} of Fe (Fig. S6). This aligns with the literature where EC_{20} after 72 h algal growth ranged from 1.1–10 mg Fe L^{-1}, depending on the water hardness, pH, and dissolved organic carbon (DOC) levels.[44] Therefore, by closely modeling environmental conditions, the algal growth inhibition test confirmed that Fe–TA@Au NPs exhibited no toxicity under environmentally realistic settings.

3.3. Mitigation of copper toxicity by Fe–TA@Au NPs

It has been well established that CuO NPs can exert toxic effects in aqueous environments *via* the release of copper ions.[8,11,45] As MPNs have the potential to act as broad-spectrum metal sequesters, owing to the free catechol and galloyl groups in the structure of the polyphenols[46] and the Cu-binding properties of TA,[47] here, Fe–TA@Au NPs were tested as a CuO NP toxicity mitigating agent. The CuO NPs used in this study had a specific surface area of 25.5 m^2 g^{-1},[12] an average hydrodynamic diameter of 298 ± 16 nm, and a ζ-potential of 21 ± 0.3 mV in ultrapure water. First, protozoa *T. thermophila* were exposed to CuO NPs to establish a dose–effect relationship in 10 mM HEPES, pH 7.4 and in ultrapure water, pH ~ 6.0 (Fig. S7a and b and Table S2). The

overall toxicity of CuO NPs appeared lower in the HEPES buffer than in water, as illustrated by ~2-fold higher EC_{50} and ~3.5-fold higher EC_{80} values in the HEPES buffer (Table S2). Although the HEPES buffer has a low Cu^{2+} complexing capacity compared to other Good's buffers[48] the reduced toxicity of CuO NPs compared to ultrapure water was either because of the lower bioavailability of dissolved copper or lower sensitivity of protozoa to toxicants in the HEPES buffer. Then, CuO NP concentrations close to the EC_{50} and EC_{80} values were used to test the effect of added Fe–TA@Au NPs on the viability of protozoa. Co-exposure of *T. thermophila* to CuO NPs and Fe–TA@Au NPs significantly mitigated the effect of CuO NPs at 100 and 125 mg L^{-1} on the viability of protozoa, both in HEPES buffer and in ultrapure water (Fig. 4a and b). In both media, the EC_{50} and EC_{80} values for CuO NPs shifted to higher values when Fe–TA@Au NPs were added to the exposure media (Fig. S8). In the HEPES buffer, compared to exposures in ultrapure water, the relative viability of protozoa was higher with added Fe–TA@Au NPs. The enhanced CuO NP toxicity mitigating properties of Fe–TA@Au NPs in the HEPES buffer than water may be attributed to the greater stability of the MPN in the HEPES buffer at pH 7.4, which allowed tris-complex formation between Fe^{3+} and TA. In contrast, in ultrapure water, with a pH ~ 6.0, Fe may have only been partially coordinated through bis-complexes,[49] resulting in a Fe–TA network of slightly different structures and pore sizes (Fig. 1f).

Fe–TA@Au NPs were also tested for their CuO NP toxicity-mitigating properties in THP-1-derived macrophage cultures. Macrophages, similar to phagocytosing protozoa, internalize nanoparticulate matter which accumulates in the lysosomes. The mechanism of CuO NP toxicity in macrophages has been proven to be the release of Cu ions, which induces protein misfolding and oxidative stress.[50] Here, CuO NPs caused dose-

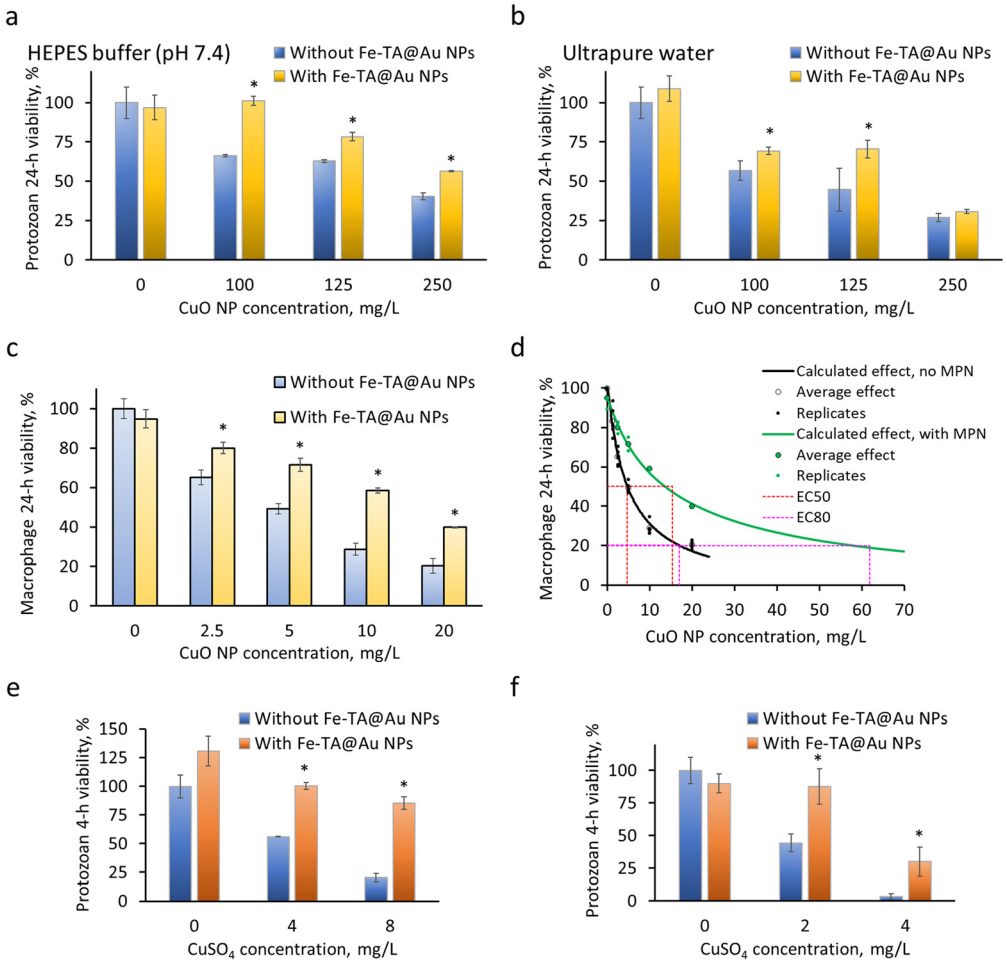

Fig. 4 Mitigation of CuO NP and $CuSO_4$ toxicity by Fe–TA@Au NPs. (a and b) Relative viability of protozoa after 24 h exposure to CuO NPs with and without Fe–TA@Au NPs at 50 mg L^{-1}. The exposure medium was either (a) 10 mM HEPES buffer, pH 7.4, or (b) ultrapure water, pH ~ 6.0. (c) Relative viability of THP-1 derived macrophages after 24 h exposure to CuO NPs with and without Fe–TA@Au NPs at 100 mg L^{-1}; exposure medium RPMI 1649. (d) Toxicity data in panel c was used to model the dose response and for the calculation of EC_{50} and EC_{80} values. (e and f) Relative viability of protozoa after 4 h exposure to $CuSO_4$ with and without Fe–TA@Au NPs in (e) 10 mM HEPES buffer, pH 7.4 or (f) ultrapure water, pH ~ 6.0. Data bars in panels a–c, e, and f represent the average values of at least three replicates, and error bars are standard deviations. Asterisks indicate significant differences ($p < 0.05$, 2-way ANOVA with Dunnett's multiple comparisons test) compared to treatment without Fe–TA@Au NPs at each respective copper concentration (panels a–c, e and f).

dependent cell death in THP-1 macrophages (Fig. 4c), with the average EC_{50} value at 4.7 mg L^{-1} and EC_{80} value at 16.9 mg L^{-1} (Fig. 4d, Table S3). The addition of Fe–TA@Au NPs to CuO NPs in the exposure medium resulted in EC_{50} and EC_{80} values that were almost an order of magnitude larger, indicating that the toxicity of CuO NPs was significantly reduced in the mixture (Fig. 4c and d, Table S3). It is worth noting that the concentration of Fe–TA@Au NPs (100 mg L^{-1}) necessary for mitigating CuO NP toxicity to THP-1 cells was twice as high as the concentration applied in the protozoan test (50 mg L^{-1}), possibly reflecting the effect of the different test media (protein-rich growth medium *versus* ultrapure water or HEPES buffer) in the charge screening and sorption of Cu^{2+}.

Based on the hypothesis that Fe–TA@Au NPs mitigated CuO NP toxicity by adsorbing Cu ions, toxicity testing was also conducted with a water-soluble salt of copper ($CuSO_4$). The EC_{50} and EC_{80} values for $CuSO_4$ to *T. thermophila* were first established (Fig. S7c and d and Table S2), and then the effects of Fe–TA@Au NPs in mitigating the toxicity of $CuSO_4$ were tested. Since the effect of $CuSO_4$ on the viability of protozoa was similar after 4 and 24 h exposures (*i.e.*, EC-values did not differ by orders of magnitude), the tests with $CuSO_4$ were conducted over 4 h. Overall, the EC_{50} values for $CuSO_4$ aligned with previously reported results under similar conditions.[11] When protozoa were co-incubated with $CuSO_4$ and Fe–TA@Au NPs, it was evident that MPNs mitigated the toxicity of $CuSO_4$ at approximate EC_{50} and EC_{80} levels of copper (4 and 8 mg L^{-1}, respectively, in HEPES buffer and 2 and 4 mg L^{-1}, respectively, in ultrapure water; Fig. 4e and f). These results suggested that the mechanism for reducing CuO NP toxicity by Fe–TA@Au NPs was, at least in part, achieved through the adsorption of Cu ions.

3.4. Underlying mechanisms of CuO NP toxicity mitigation by Fe–TA@Au NPs – reduction of bioavailable Cu and intracellular ROS

To confirm the hypothesis that Fe–TA@Au NPs rescued protozoa from the lethal effect of CuO NPs by sequestering dissolved Cu ions, bioavailable Cu was quantified in the test medium (ultrapure water) after the exposure of protozoa to either CuO NPs alone or with Fe–TA@Au NPs. $CuSO_4$, a water-soluble Cu-salt, was used as a reference for 100% bioavailable copper in the exposure medium: it was confirmed experimentally that the test solution of $CuSO_4$ at the nominal concentration of 2 mg Cu L^{-1} contained on average 2 mg L^{-1} of bioavailable copper (Fig. 5a). In the test suspension where protozoa were exposed to CuO NPs at 125 mg L^{-1} (close to the EC_{50} value), the average bioavailable copper content was 1.8 mg L^{-1}. Similar bioavailable Cu concentrations (around 2 mg L^{-1}) at the EC_{50} levels of both $CuSO_4$ and CuO NPs suggest that the toxicity of CuO NPs was mediated through released Cu ions, consistent with previous findings obtained under similar experimental conditions.[11] The addition of Fe–TA@Au NPs to either $CuSO_4$ or CuO NPs in the protozoan exposure medium reduced bioavailable copper content by about 2 and 1.5 fold, respectively, to the level of ~1 mg Cu L^{-1}. Based on the toxicity experiments, there was a negligible effect at 1 mg Cu L^{-1} on protozoan viability (Fig. S7d). Thus, Fe–TA@Au NPs reduced the concentration of bioavailable copper in the $CuSO_4$ solution and CuO NP suspension below lethal copper levels.

Copper binding by Fe–TA@Au NPs under abiotic conditions in ultrapure water was also confirmed by an analytical method – TRXF spectroscopy, which confirmed similar adsorbed quantities of Cu (Fig. 5b). Further, the mode of Cu adsorption by Fe–TA@Au NPs was explored through adsorption experiments, and the experimental data were fitted to the Langmuir and Freundlich models (Fig. 5c and S9). The adsorption isotherms suggested that both monolayer and multilayer adsorption mechanisms were thermodynamically favorable, as indicated by the high correlation coefficients (R^2, Table 1), with a higher tendency for multilayer adsorption following the Freundlich isotherm model (R^2 = 0.991). Further, the Freundlich isotherm $1/n$ value <1 indicates a favorable spontaneous adsorption process, crucial for the removal of metals, especially at low concentrations.[51] The Freundlich constant (K_F) value (72.8)

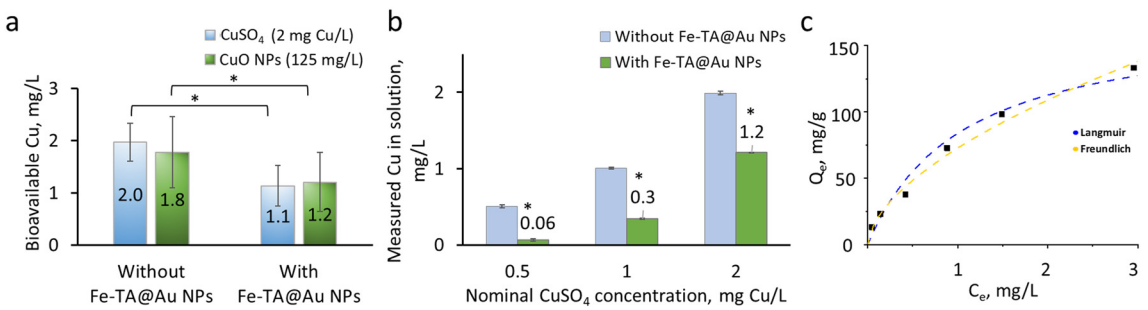

Fig. 5 Copper adsorption by Fe–TA@Au NPs. (a) Bioavailable copper in the toxicity test medium after exposure of protozoa to $CuSO_4$ at 2 mg Cu L^{-1} or CuO NPs at 125 mg L^{-1} (EC_{50} levels) in ultrapure water for 2 h; the asterisks indicate significant differences between the treatments with and without Fe–TA@Au NPs. (b) Copper concentrations in $CuSO_4$ solutions in ultrapure water before and after the addition of Fe–TA@Au NPs; the incubation time was 2 h, and the asterisks indicate a significant difference ($p > 0.05$) from the respective Cu solutions without Fe–TA@Au NPs. (c) Adsorption isotherms were modeled based on Langmuir and Freundlich equations; the black squares represent the experimental data. The adsorbent concentration was 30.4 mg L^{-1} of Fe–TA network; temperature 22 °C, solution pH 6.0, and mixing time 2 h.

Table 1 Adsorption isotherm constants for the adsorption of Cu^{2+} by the Fe–TA network (the active component of Fe–TA@Au NPs)

Langmuir model			Freundlich model		
K_L (L mg^{-1})	Q_M (mg g^{-1})	R^2	K_F	$1/n$	R^2
0.9508	172	0.925	72.8	0.58	0.991

obtained here for Cu^{2+} adsorption by Fe–TA@Au NPs was similar to the respective value reported for a common metal–organic framework (MOF) ZIF-8,[52] suggesting comparable adsorption affinity of these materials for Cu^{2+}. The maximum adsorption capacity (Q_M) of Fe–TA@Au NPs (172 mg g^{-1} Fe–TA), calculated based on the Langmuir isotherm, is comparable to other adsorbents used for Cu^{2+} binding, showing the respective values in the range of 45–398 mg g^{-1}.[53] The Q_M of Fe–TA@Au NPs was higher than the maximum Cu^{2+} adsorption capacity of the microsized Zr–TA MPN (135 mg g^{-1}),[46] suggesting that MPN nanocomposites enabled improved Cu adsorption compared to microsized MPN materials. Overall, both physical and chemical adsorption of Cu^{2+} may have occurred considering the porous 3D structure of Fe–TA MPNs and negatively charged hydroxyl groups of TA available for forming complexes with Cu^{2+} *via* coordination bonds.[46]

To evaluate the potential ion exchange mechanism involved in Cu^{2+} adsorption by Fe–TA MPN, we measured Fe ions released from the Fe–TA@Au NPs in $CuSO_4$ solutions using TRXF spectroscopy. The Fe–TA@Au NPs were mixed with $CuSO_4$ at molar ratios of Fe : Cu at 2.6, 3.5 and 4.4. The Fe concentrations released into $CuSO_4$ solutions were less than 10% of the Fe content in the Fe–TA@Au NPs and did not increase with higher Cu^{2+} concentrations. These results suggest that Cu^{2+} binding likely occurs through accessible hydroxyl groups in the TA molecules rather than by replacing Fe^{3+} in the MPN structure. This mechanism is similar to what has been proposed for Zr–TA MPNs.[46,54]

Since TA is a compound with excellent antioxidative properties, we also considered the possibility of its contribution to mitigating Cu toxicity by reducing the level of ROS in cells. To test this hypothesis, we first determined the ability of Fe–TA@Au NPs to reduce intracellular ROS in protozoa. The results showed that Fe–TA@Au NPs were effective in mitigating H_2O_2-induced excessive ROS in the protozoan cells (Fig. 6a–g). Fluorescence microscopy demonstrated intense green fluorescence in H_2O_2-treated cells, indicative of high levels of intracellular ROS (Fig. 6b and e), in contrast to control cells that were in ultrapure water and exhibited no fluorescence upon DCFH-DA staining (Fig. 6a and d). A considerably lower number of green fluorescing cells was visible in the sample where H_2O_2

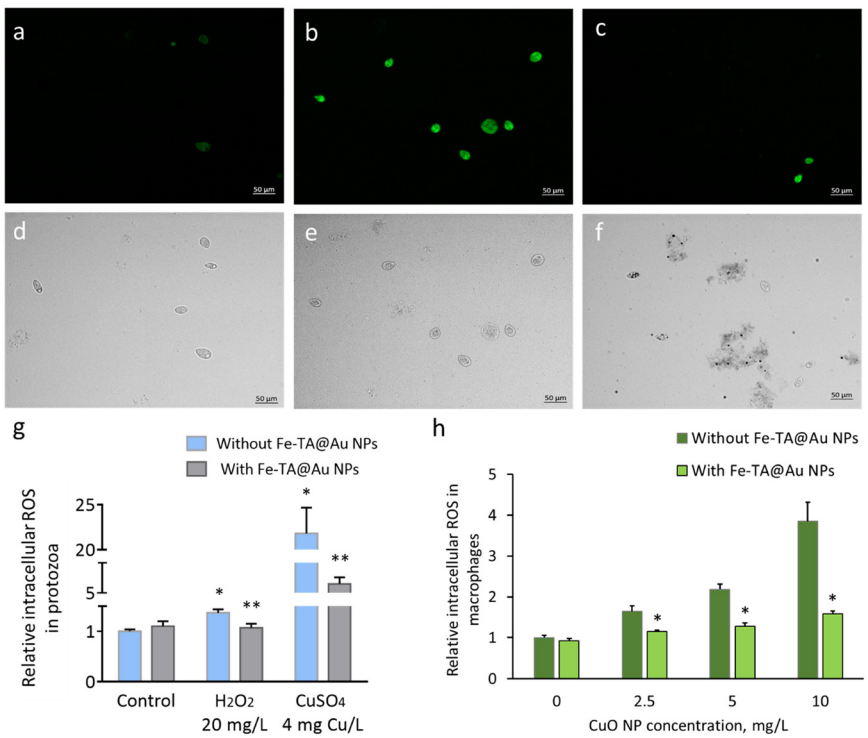

Fig. 6 Reduction of intracellular ROS by Fe–TA@Au NPs. (a–c) Fluorescence and (d–f) bright-field microscopy images of protozoa incubated for 4 h in (a and d) ultrapure water, (b and e) 20 mg L^{-1} H_2O_2 solution in water, and (c and f) 20 mg L^{-1} H_2O_2 solution supplemented with Fe–TA@Au NPs; scale bars: 50 μm. (g) Quantitative analysis of intracellular ROS in protozoa after a 4 h exposure to 20 mg L^{-1} H_2O_2 or $CuSO_4$ at 4 mg Cu L^{-1} with and without Fe–TA@Au NPs. * – significant difference from the control cells in water, ** – significant difference from the treatment without Fe–TA@Au NPs, $p < 0.05$. (h) Relative intracellular ROS levels in THP-1-derived macrophages after a 24 h exposure to CuO NPs with and without Fe–TA@Au NPs in RPMI 1649 medium; asterisks indicate significant difference from the respective treatment without Fe–TA@Au NPs, $p < 0.05$.

was supplemented with Fe–TA@Au NPs, suggesting suppressed ROS production in protozoa (Fig. 6c and f). A quantitative analysis of green fluorescence of the ROS-indicative stain confirmed the visual observations: Fe–TA@Au NPs mitigated intracellular ROS production in H_2O_2-treated cells as well as in Cu^{2+}-treated cells (Fig. 6g). Pure tannic acid at the same concentration present in Fe–TA@Au NPs was also effective in reducing H_2O_2-induced ROS levels in protozoa (data not shown), suggesting that TA was mainly responsible for the antioxidative properties of Fe–TA@Au NPs. To confirm the ROS-mitigating effect of Fe–TA@Au NPs in a human-relevant *in vitro* cell model, intracellular ROS was quantified in THP-1-derived macrophages after exposure to CuO NPs with and without the addition of Fe–TA@Au NPs. Fe–TA@Au NPs significantly reduced the intracellular ROS close to the control levels (Fig. 6h), demonstrating the efficiency of the MPN nanocomposites in different cellular systems and exposure conditions.

To assess the impact of nanocomposite aging on the effectiveness of Fe–TA@Au NPs in reducing copper toxicity, we conducted tests with protozoa exposed to $CuSO_4$. These tests were performed with and without Fe–TA@Au NPs that had been stored at 4 °C in the dark for up to 6 days. The results indicated that Fe–TA@Au NPs maintained their efficiency at least after three days of aging, reducing $CuSO_4$ toxicity in the 4 h *T. thermophila* toxicity test at a comparable level to unaged Fe–TA@Au NPs (Fig. S10a). After six days of aging, the efficiency decreased to 78% in the 4 h exposure test. However, when protozoa were exposed to Cu for 24 h, the Fe–TA@Au NPs retained their toxicity-reducing efficiency after six days of aging (Fig. S10b). This suggests that aged MPN nanocomposites were sufficiently effective when allowed to act over a longer time. This is significant because Cu toxicity often correlates with the exposure duration, making it crucial to mitigate toxicity over an extended period.

4. Conclusions

A recent review of trends in nanomaterial production volumes and applications by sector has identified that nanomaterials actively developed for use in the agricultural industry are primarily copper-based.[2] Although the use of nanomaterials in agriculture is still in its early stages, their direct application in the environment could lead to potential ecological and human health risks. Therefore, developing effective measures to mitigate the toxicity of copper nanomaterials is a timely effort. Here, Fe–TA-based nanocomposite materials were demonstrated to perform as excellent CuO NP toxicity mitigating agents, applicable in freshwater unicellular organisms as well as human macrophages. Superior biocompatibility and relatively high maximum adsorption capacity for Cu^{2+} (172 mg g^{-1} Fe–TA MPN) indicate great potential for these porous materials in various Cu-adsorbing applications both in environmental and human health-related fields. Notably, the Fe–TA@Au NPs efficiently mitigated Cu toxicity at nanocomposite concentrations that were relatively low in the TA content (15–30 mg TA L^{-1}). This is significant given the frequently excessive TA contents of industrial wastewater, which must be removed before biological water treatment to prevent toxicity to sludge organisms.[55] In scaled-up environmental applications, the Au NP cores used in the current study can be substituted for more cost-effective SiO_2 or iron oxide NPs. The latter materials would render MPN nanocomposites magnetic to facilitate their removal from the aqueous media. Further, the MPN nanocomposites may be used in conjunction with membrane substrates for more effective Cu adsorption.

Author contributions

Anett Välimets: methodology, investigation, data curation, formal analysis, visualization, writing – original draft; Danylo Merzhyievskyi: data curation, methodology, investigation, formal analysis, visualization, writing – original draft; Ilona Juvonen: investigation, data curation, formal analysis, visualization; Karin Valmsen: methodology, investigation, data curation, formal analysis; Isabelle Worms: methodology, investigation, data curation, formal analysis, visualization, writing – original draft, writing – review & editing; Vera I. Slaveykova: resources, supervision, writing – review & editing; Asya Drenkova-Tuhtan: formal analysis, methodology, writing – review & editing; Nicholas Andrikopoulos: formal analysis, methodology, writing – review & editing; Pu Chun Ke: conceptualization, writing – review & editing; Anne Kahru: resources, writing – review & editing; Monika Mortimer: conceptualization, funding acquisition, project administration, supervision, writing – review & editing.

Conflicts of interest

The authors declare no conflict of interest.

Data availability

The data supporting this article have been included as part of the supplementary information (SI).

Supplementary information: includes additional methods, figures and tables presenting results and method calibration data. See DOI: https://doi.org/10.1039/d5en00428d.

Acknowledgements

This research was funded by the Estonian Research Council (PRG2188 and PRG2595) and the NAMUR+ core facility (TT13). The authors acknowledge the use of the ATR-FTIR instrument (Shimadzu IRAffinity-1S equipped with a Specac Quest ATR accessory) at Tallinn University of Technology, School of Engineering, Department of Materials and Environmental Technology, Laboratory of Biopolymer Technology. The authors thank Kaja Kasemets for help with THP-1 cell culturing and toxicity testing, Maarja Otsus for confocal fluorescence microscopy, and Heiki Vija for assistance with TXRF spectrometry (S2 PICOFOX, Bruker).

References

1 *Report Nanomaterials Market Size, Share & Trends Analysis Report By Product, By Application, By Region, And Segment Forecasts, 2020–2027*, Report ID: GVR-4-68038-565-6, Grand View Research, San Francisco, USA, 2020.
2 A. A. Keller, A. Ehrens, Y. Zheng and B. Nowack, Developing trends in nanomaterials and their environmental implications, *Nat. Nanotechnol.*, 2023, **18**(8), 834–837.
3 J. Zhou, Y. Wang, N. Zuverza-Mena, C. O. Dimkpa and J. C. White, Copper-based materials as an effective strategy for improving drought resistance in soybean (*Glycine max*) at the reproductive stage, *ACS Agric. Sci. Technol.*, 2024, **4**(7), 735–746.
4 W. Huang, F. Tao, F. Li, M. Mortimer and L.-H. Guo, Antibacterial nanomaterials for environmental and consumer product applications, *NanoImpact*, 2020, **20**, 100268.
5 S. Kalidhasan, M.-S. Kang, J. Choi and H.-Y. Lee, Smart and responsive nano copper oxide–PDMS composite for "three-in-one" synergistic adsorptive–oxidative / reductive degradation of the persistence of organic pollutants, elimination of nanoparticles and heavy metal ion, *J. Cleaner Prod.*, 2024, **469**, 143150.
6 O. Bondarenko, K. Juganson, A. Ivask, K. Kasemets, M. Mortimer and A. Kahru, Toxicity of Ag, CuO and ZnO nanoparticles to selected environmentally relevant test organisms and mammalian cells *in vitro*: a critical review, *Arch. Toxicol.*, 2013, **87**(7), 1181–1200.
7 R. J. Miller, A. S. Adeleye, H. M. Page, L. Kui, H. S. Lenihan and A. A. Keller, Nano and traditional copper and zinc antifouling coatings: metal release and impact on marine sessile invertebrate communities, *J. Nanopart. Res.*, 2020, **22**(5), 129.
8 A. Ivask, K. Juganson, O. Bondarenko, M. Mortimer, V. Aruoja, K. Kasemets, I. Blinova, M. Heinlaan, V. Slaveykova and A. Kahru, Mechanisms of toxic action of Ag, ZnO and CuO nanoparticles to selected ecotoxicological test organisms and mammalian cells *in vitro*: a comparative review, *Nanotoxicology*, 2014, **8**(Suppl 1), 57–71.
9 K. Juganson, M. Mortimer, A. Ivask, K. Kasemets and A. Kahru, Extracellular conversion of silver ions into silver nanoparticles by protozoan *Tetrahymena thermophila*, *Environ. Sci.: Processes Impacts*, 2013, **15**(1), 244–250.
10 K. Juganson, M. Mortimer, A. Ivask, S. Pucciarelli, C. Miceli, K. Orupold and A. Kahru, Mechanisms of toxic action of silver nanoparticles in the protozoan *Tetrahymena thermophila*: From gene expression to phenotypic events, *Environ. Pollut.*, 2017, **225**, 481–489.
11 M. Mortimer, K. Kasemets and A. Kahru, Toxicity of ZnO and CuO nanoparticles to ciliated protozoa *Tetrahymena thermophila*, *Toxicology*, 2010, **269**(2–3), 182–189.
12 M. Mortimer, K. Kasemets, M. Vodovnik, R. Marinsek-Logar and A. Kahru, Exposure to CuO nanoparticles changes the fatty acid composition of protozoa *Tetrahymena thermophila*, *Environ. Sci. Technol.*, 2011, **45**(15), 6617–6624.
13 A. Gallego, A. Martín-González, R. Ortega and J. C. Gutiérrez, Flow cytometry assessment of cytotoxicity and reactive oxygen species generation by single and binary mixtures of cadmium, zinc and copper on populations of the ciliated protozoan *Tetrahymena thermophila*, *Chemosphere*, 2007, **68**(4), 647–661.
14 A. Käkinen, O. Bondarenko, A. Ivask and A. Kahru, The effect of composition of different ecotoxicological test media on free and bioavailable copper from $CuSO_4$ and CuO nanoparticles: Comparative evidence from a Cu-selective electrode and a Cu-biosensor, *Sensors*, 2011, **11**(11), 10502–10521.
15 H. Naatz, S. Lin, R. Li, W. Jiang, Z. Ji, C. H. Chang, J. Köser, J. Thöming, T. Xia, A. E. Nel, L. Mädler and S. Pokhrel, Safe-by-design CuO nanoparticles via Fe-doping, Cu–O bond length variation, and biological assessment in cells and zebrafish embryos, *ACS Nano*, 2017, **11**(1), 501–515.
16 P. Chen, B. A. Powell, M. Mortimer and P. C. Ke, Adaptive interactions between zinc oxide nanoparticles and *Chlorella* sp, *Environ. Sci. Technol.*, 2012, **46**(21), 12178–12185.
17 L. M. Stevenson, H. Dickson, T. Klanjscek, A. A. Keller, E. McCauley and R. M. Nisbet, Environmental feedbacks and engineered nanoparticles: mitigation of silver nanoparticle toxicity to *Chlamydomonas reinhardtii* by algal-produced organic compounds, *PLoS One*, 2013, **8**(9), e74456.
18 T. Gräf, V. Koch, J. Köser, J. Fischer, C. Tessarek and J. Filser, Biotic and abiotic interactions in freshwater mesocosms determine fate and toxicity of CuO nanoparticles, *Environ. Sci. Technol.*, 2023, **57**(33), 12376–12387.
19 Z. Li, G. Lu, D. Du and D. Zhao, Harnessing low-cost adsorbents for removal of heavy metals and metalloids in contaminated water: Progress in the past decade and future perspectives, *J. Cleaner Prod.*, 2025, **518**, 145845.
20 Y. Wang, X. Liang, N. Andrikopoulos, H. Tang, F. He, X. Yin, Y. Li, F. Ding, G. Peng, M. Mortimer and P. C. Ke, Remediation of metal oxide nanotoxicity with a functional amyloid, *Adv. Sci.*, 2024, **11**(23), 2310314.
21 W. Xie, Z. Guo, L. Zhao and Y. Wei, Metal-phenolic networks: facile assembled complexes for cancer theranostics, *Theranostics*, 2021, **11**(13), 6407–6426.
22 H. Geng, Q. Z. Zhong, J. Li, Z. Lin, J. Cui, F. Caruso and J. Hao, Metal ion-directed functional metal-phenolic materials, *Chem. Rev.*, 2022, **122**(13), 11432–11473.
23 FDA, *GRAS Substances (SCOGS) Database*, https://www.fda.gov/food/generally-recognized-safe-gras/gras-substances-scogs-database, In 1972–1980.
24 M. P. Ko and C. J. Huang, A versatile approach to antimicrobial coatings via metal-phenolic networks, *Colloids Surf., B*, 2020, **187**, 110771.
25 Y. Ju, C. Cortez-Jugo, J. Chen, T.-Y. Wang, A. J. Mitchell, E. Tsantikos, N. Bertleff-Zieschang, Y.-W. Lin, J. Song, Y. Cheng, S. Mettu, M. A. Rahim, S. Pan, G. Yun, M. L. Hibbs, L. Y. Yeo, C. E. Hagemeyer and F. Caruso, Engineering of nebulized metal–phenolic capsules for controlled pulmonary deposition, *Adv. Sci.*, 2020, **7**(6), 1902650.

26 T. Zeng, X. Zhang, Y. Guo, H. Niu and Y. Cai, Enhanced catalytic application of Au@polyphenol-metal nanocomposites synthesized by a facile and green method, *J. Mater. Chem. A*, 2014, **2**(36), 14807–14811.
27 W. Zhang, A. J. Christofferson, Q. A. Besford, J. J. Richardson, J. Guo, Y. Ju, K. Kempe, I. Yarovsky and F. Caruso, Metal-dependent inhibition of amyloid fibril formation: synergistic effects of cobalt-tannic acid networks, *Nanoscale*, 2019, **11**(4), 1921–1928.
28 R. Gasco, I. A. M. Worms, D. Santos and V. I. Slaveykova, Asymmetric flow field-flow fractionation for comprehensive characterization of hetero-aggregates made of nano-silver and extracellular polymeric substances, *J. Chromatogr. A*, 2025, **1739**, 465507.
29 R. Gasco, I. A. M. Worms, A. Kantarciyan and V. I. Slaveykova, Diatom-derived extracellular polymeric substances form eco-corona and enhance stability of silver nanoparticles, *Environ. Sci.: Nano*, 2024, **11**(10), 4138–4150.
30 A. J. Brenner and E. D. Harris, A quantitative test for copper using bicinchoninic acid, *Anal. Biochem.*, 1995, **226**(1), 80–84.
31 M. Mortimer, T. Kefela, A. Trinh and P. A. Holden, Uptake and depuration of carbon- and boron nitride-based nanomaterials in the protozoa *Tetrahymena thermophila*, *Environ. Sci.: Nano*, 2021, **8**(12), 3613–3628.
32 V. Aruoja, S. Pokhrel, M. Sihtmae, M. Mortimer, L. Madler and A. Kahru, Toxicity of 12 metal-based nanoparticles to algae, bacteria and protozoa, *Environ. Sci.: Nano*, 2015, **2**(6), 630–644.
33 E. Vindimian, https://www.normalesup.org/~vindimian/en_index.html.
34 OECD, *Test No. 201: Freshwater Alga and Cyanobacteria, Growth Inhibition Test, OECD Guidelines for the Testing of Chemicals, Section 2*, OECD Publishing, Paris, 2011, DOI: 10.1787/9789264069923-en.
35 A. Ivask, T. Rõlova and A. Kahru, A suite of recombinant luminescent bacterial strains for the quantification of bioavailable heavy metals and toxicity testing, *BMC Biotechnol.*, 2009, **9**(1), 41.
36 T. Hendel, M. Wuithschick, F. Kettemann, A. Birnbaum, K. Rademann and J. Polte, In situ determination of colloidal gold concentrations with UV-vis spectroscopy: limitations and perspectives, *Anal. Chem.*, 2014, **86**(22), 11115–11124.
37 H. Luo, S. Zhang, X. Li, X. Liu, Q. Xu, J. Liu and Z. Wang, Tannic acid modified Fe_3O_4 core–shell nanoparticles for adsorption of Pb^{2+} and Hg^{2+}, *J. Taiwan Inst. Chem. Eng.*, 2017, **72**, 163–170.
38 Y.-M. Li, X. L. Miao, Z. Wei, J. Cui, S. Y. Li, R. Han, Y.-K. Zhang and W. Wei, Iron-tannic acid nanocomplexes: facile synthesis and application for removal of methylene blue from aqueous solution, *Dig. J. Nanomater. Biostruct.*, 2016, **11**, 1045–1061.
39 M. Mortimer, A. Kahru and V. I. Slaveykova, Uptake, localization and clearance of quantum dots in ciliated protozoa *Tetrahymena thermophila*, *Environ. Pollut.*, 2014, **190**, 58–64.
40 J. R. Nilsson, On food vacuoles in *Tetrahymena pyriformis* GL, *J. Protozool.*, 1977, **24**(4), 502–507.
41 V. R. Dayeh, D. H. Lynn and N. C. Bols, Cytotoxicity of metals common in mining effluent to rainbow trout cell lines and to the ciliated protozoan, *Tetrahymena thermophila*, *Toxicol. In Vitro*, 2005, **19**(3), 399–410.
42 X. Li, H. Liu, Z. Lin, J. J. Richardson, W. Xie, F. Chen, W. Lin, F. Caruso, J. Zhou and B. Liu, Cytoprotective metal-phenolic network sporulation to modulate microalgal mobility and division, *Adv. Sci.*, 2024, **11**(3), e2308026.
43 A. Cid, R. Prado, C. Rioboo, P. Suarez-Bregua and C. Herrero, Use of Microalgae as Biological Indicators of Pollution: Looking for New Relevant Cytotoxicity Endpoints, in *Microalgae: Biotechnology, Microbiology and Energy*, ed. M. N. Johnsen, Nova Science Publishers, New York, 2012, pp. 311–323.
44 A. S. Cardwell, P. H. Rodriguez, W. A. Stubblefield, D. K. DeForest and W. J. Adams, Chronic toxicity of iron to aquatic organisms under variable pH, hardness, and dissolved organic carbon conditions, *Environ. Toxicol. Chem.*, 2023, **42**(6), 1371–1385.
45 V. Aruoja, H.-C. Dubourguier, K. Kasemets and A. Kahru, Toxicity of nanoparticles of CuO, ZnO and TiO_2 to microalgae *Pseudokirchneriella subcapitata*, *Sci. Total Environ.*, 2009, **407**(4), 1461–1468.
46 M. A. Rahim, G. Lin, P. P. Tomanin, Y. Ju, A. Barlow, M. Björnmalm and F. Caruso, Self-assembly of a metal–phenolic sorbent for broad-spectrum metal sequestration, *ACS Appl. Mater. Interfaces*, 2020, **12**(3), 3746–3754.
47 P. Kraal, B. Jansen, K. G. J. Nierop and J. M. Verstraten, Copper complexation by tannic acid in aqueous solution, *Chemosphere*, 2006, **65**(11), 2193–2198.
48 N. E. Good, G. D. Winget, W. Winter, T. N. Connolly, S. Izawa and R. M. Singh, Hydrogen ion buffers for biological research, *Biochemistry*, 1966, **5**(2), 467–477.
49 Z. Lin, H. Liu, J. J. Richardson, W. Xu, J. Chen, J. Zhou and F. Caruso, Metal–phenolic network composites: from fundamentals to applications, *Chem. Soc. Rev.*, 2024, **53**(22), 10800–10826.
50 G. Gupta, F. Cappellini, L. Farcal, R. Gornati, G. Bernardini and B. Fadeel, Copper oxide nanoparticles trigger macrophage cell death with misfolding of Cu/Zn superoxide dismutase 1 (SOD1), *Part. Fibre Toxicol.*, 2022, **19**(1), 33.
51 J. Luo, D. Yu, K. D. Hristovski, K. Fu, Y. Shen, P. Westerhoff and J. C. Crittenden, Critical review of advances in engineering nanomaterial adsorbents for metal removal and recovery from water: mechanism identification and engineering design, *Environ. Sci. Technol.*, 2021, **55**(8), 4287–4304.
52 W. Yang, Y. Kong, H. Yin and M. Cao, Study on the adsorption performance of ZIF-8 on heavy metal ions in water and the recycling of waste ZIF-8 in cement, *J. Solid State Chem.*, 2023, **326**, 124217.

53 C. Wu, K.-H. Low and V. K.-M. Au, Efficient removal and sensing of copper(II) ions by alkaline earth metal-based metal–organic frameworks, *J. Solid State Chem.*, 2023, **322**, 123936.
54 S. Chen, L. Wang, W. Ni and H. Qiu, The effect of coordination state on the activity of TA-Zr supramolecular networks for heavy metals removal from water, *React. Funct. Polym.*, 2025, **210**, 106190.
55 J. Perkowski, U. Dawidow and W. K. Jóźwiak, Advanced oxidation of tannic acid in aqueous solution, *Ozone: Sci. Eng.*, 2003, **25**(3), 199–209.